Comparative Evaluation of Positioning Methods for Finite Element Human Body Models in Virtual Crash Testing: Implications for Mesh Quality and Injury Prediction

Simona Roka, Pablo Lozano, Sandeep Dudhade, Amol Jaware

Abstract With the integration of virtual testing protocols in Euro NCAP 2026, utilising Human Body Models' (HBMs) standardised positioning methodologies will be essential for reliable injury prediction. This study evaluates four distinct positioning methods for finite element HBMs and their effects on mesh quality and injury outcomes. The following methods were investigated: (A) morphing with a commercial de-penetration tool; (B) articulated HBM with simulation-based seat compression; (C) marionette positioning with cable-controlled joint movement; and (D) advanced marionette with simultaneous seat compression using deformable HBM. Three models were evaluated: THUMS AM50 v4.1, THUMS AM50 v6.1, and VIVA+ M50 v2.0.1, using frontal crash simulations. Mesh quality degradation following positioning remained minimal (<1% in most cases), with morphing methods maintaining quality closest to baseline configurations. Kinematic analysis revealed negligible differences in gross occupant motion across all methods, with identical starting positions and near-identical trajectories during the loading phase. Approximately 40% of the 19 injury metrics evaluated demonstrated model-dependent positioning method effectiveness, with head injury criterion (HIC) varying by 51.9–102.8% of applied limits in THUMS v4.1 while remaining stable in VIVA+ (CV <1%). Tibia bending moments showed the highest lower extremity variability (CV: 15–22%), and chest rib fracture risk for elderly occupants approached critical levels (64.8–73.0% of injury limit) with less method sensitivity than younger age groups. These findings reveal that while HBM positioning methods yield comparable mesh quality and kinematics, injury metric predictions exhibit non-negligible method-specific and model-dependent variations.

Keywords Human Body Models, Injury prediction, Mesh quality, Positioning methodology, Virtual testing.

I. INTRODUCTION

Finite element (FE) human body models (HBMs) have become increasingly important tools in automotive safety research, providing detailed insights into occupant response and injury risk in crash scenarios. However, positioning models while preserving mesh quality remains a significant challenge [1].

The fundamental challenge in HBM positioning comes from the need to transform baseline model postures, typically delivered in standardised configurations, into postures representative of real-world occupants. This transformation must account for complex anatomical constraints while preserving the FE mesh quality necessary for reliable crash simulations [2]. Traditional approaches have included simulation-based methods, pre-calculated databases, and various interpolation techniques, each presenting distinct trade-offs between computational efficiency, anatomical fidelity, and mesh quality preservation [1][3].

Throughout the evolution of positioning methodologies, mesh quality preservation has appeared as a critical factor affecting simulation accuracy and stability. The PIPER project emphasised that models must be 'positionable', meaning soft tissue must follow joint motion in a manner that preserves element quality without requiring remeshing [1]. Beillas *et al.* [1] noted that all evaluated interpolation methods provided acceptable results for stature and anthropometry changes when control points were appropriately selected, but emphasised that mesh quality considerations must guide method selection [1].

Element skewness has been consistently identified as particularly sensitive to positioning transformations [2-3]. Zhang *et al.* [4] carefully monitored Jacobian determinants across their morphing process, establishing thresholds of 0.3 for solid elements and 0.7 for shell elements as quality metrics. Tang *et al*. [2] addressed mesh quality through their morph-contact algorithm, which explicitly detected and eliminated penetrations before applying optimisation-based refinement. Chen and Li [3] took a more systematic approach by implementing

S. Roka (e-mail: simona.roka@idiada.com) is a Senior Engineer at Applus IDIADA and a PhD student at Comillas Pontifical University, Spain. P. Lozano is a Project Engineer at Applus IDIADA. S. Dudhade is a Manager and A. Jaware a former Project Engineer at IDIADA India.

automated post-processing mesh repair to correct defective nodes. Their results demonstrated that 85% improvement in elements with a Jacobian below 0.3 could be achieved, with the complete elimination of negative volume elements in certain cases [3].

Despite these advances, questions remain about the influence of positioning methodology on injury-prediction outcomes and the relationship between positioning-induced mesh quality degradation and simulation fidelity. Some recent studies have demonstrated that positioning can be achieved rapidly while maintaining acceptable mesh quality metrics, but the sensitivity of injury parameters to different positioning methods has not been systematically characterised across multiple HBMs.

The present study addresses these questions by evaluating the influence of occupant positioning methodology on both injury prediction outcomes and mesh quality in FE HBM simulations. Multiple positioning approaches that are being used in industry were compared across different HBM models to quantify the sensitivity of injury metrics to the selection of positioning methods and to characterise the degradation patterns of mesh quality associated with different positioning techniques.

II. METHODS

Three 50th percentile adult male HBMs were employed in this study: THUMS AM50 v4.1, THUMS AM50 v6.1, and VIVA+ M50 v2.0.1. All models were obtained in their initial seating configurations and required positioning into the vehicle occupant compartment.

Positioning methods

Four different approaches were investigated to position the HBMs in the vehicle environment and to resolve penetrations between the HBMs and the seat. The methods differed in their positioning strategy and in the procedure used to resolve seat-HBM intersections. The investigated approaches included morphing-based positioning, simulation-based positioning using the marionette method, and seat de-penetration using either morphing or pre-simulation.

Method A

The HBM was positioned using morphing tools in the commercial pre-processor ANSA v24.1.2 (Beta CAE, Greece), specifically the Human Body Model Articulation tool, using the metadata provided for each HBM. The entire HBM was first translated to the target H-point location. Subsequently, individual body segments were adjusted using biofidelic positioning options provided by the pre-processor.

The posture was configured to represent a typical driver posture for a frontal impact scenario. The hands were placed in a quarter-to-three position on the steering wheel with the thumbs in contact with the rim. The right foot was positioned on the accelerator pedal in an undepressed state, while the left foot was placed on the footrest.

Intersections between the HBM and the seat were resolved using the seat de-penetration tool of the pre-processor. A morphing analysis was applied to deform the seat mesh locally to eliminate penetrations between the seat and the HBM.

Method B

The HBM positioning procedure was identical to that described in *Method A*, but seat de-penetration was achieved via a short pre-simulation rather than by morphing.

For this purpose, the external shell components of the HBM were modelled as a rigid body to maintain the HBM's posture during morphing using the pre-processor tool. During the pre-simulation, a boundary-prescribed motion was applied to the rigid HBM, moving it toward the seat. This allowed the seat elements to deform naturally under contact interaction with the HBM rigid shell. After completion of the pre-simulation, the deformed seat node coordinates were extracted and substituted into the original model file, resulting in a seat geometry adapted to the HBM position. Pre-stress in the seat was applied using the *INITIAL_REFERENCE_GEOMETRY card in LSDYNA, with the undeformed mesh of the seat as the reference. This pre-stress was used in methods B, C and D.

Method C

The HBM was positioned using the marionette method via simulation. This simulation was configured using the Human Body Model Marionette tool available in ANSA. This method performs positioning via a simulation-based approach, reducing potential intersections that may occur in the HBM when positioning is done purely by morphing.

In this approach, virtual cables are generated between the bones of the HBM in the default model posture provided by the model developer and nodes corresponding to the desired target posture that are fixed in space. The cables are pre-tensioned and apply force that gradually moves the model towards the target posture.

In the present study, a cable constant force of 0.5 kN and a cable and global damping coefficient of 0.3 were used. The cables were attached primarily to rigid skeletal structures of the HBM, such as bones, and were used to move the limbs and body segments to the target configuration. Gravity was applied during the pre-simulation to account for realistic soft-tissue deformation. The cable parameters can be adjusted to improve simulation stability and computational efficiency. Seat de-penetration was subsequently performed using the pre-simulation procedure described in *Method B*.

Method D

This represents an extension of the marionette positioning approach. In addition to positioning the HBM through simulation, the surrounding environment, including the seat and carpet, was also included in the pre-simulation and allowed to move during the positioning process. In this method, the seat and carpet components were initially offset from their original positions in the model. A prescribed boundary motion was then applied to move these components back to their nominal positions during the simulation. While the environment was moving, the HBM was simultaneously positioned using the marionette cable system described in *Method C*. This combined motion allowed the seat and surrounding components to deform naturally as the HBM settled into the seat. Gravity was active throughout the simulation.

At the end of the simulation, the method produced a positioned HBM with minimal intersections with the vehicle environment and a seat geometry that had been automatically de-penetrated through physical deformation.

TABLE I

POSITIONING METHODS

Parameter	Method A	Method B	Method C	Method D
HBM positioning approach	Morphing	Morphing	Marionette simulation	Marionette simulation
Seat de-penetration approach	Morphing	Pre-simulation	Pre-simulation	Coupled simulation
Pre-simulation duration (HBM)	—	—	300 ms	300 ms
Pre-simulation duration (seat)	—	60 ms	60 ms	(included in 300 ms)
Gravity	—	No	Yes	Yes
Cable Force (F0)	—	—	200 N	200 N
Damping Constant (DC)	—	—	0.3 N.ms/mm	0.3 N.ms/mm
Global Damping Coefficient (VALDMP)	—	—	0.001	0.001

Crash vehicle model and boundary conditions

The Honda Accord open-source frontal offset impact model [5] was selected for the crash simulations. Steering wheel, floor, dashboard, CCB, and firewall assemblies are isolated from this model for our injury prediction performance investigation simulations. Intrusions of the dashboard, steering wheel, floor, and firewall were prescribed using the *BOUNDARY_PRESCRIBED_MOTION keyword. All model assemblies were defined as rigid bodies, except for the floor structure surrounding the driver's foot region, which was modelled as deformable.

A velocity pulse was applied in the positive X-direction to the body-in-white (BIW) at a location beneath the driver's seat. All remaining degrees-of-freedom of the BIW were constrained.

The study used the open-source validated driver seat model developed within Project VIRTUAL [6]. This seat model represents the front passenger seat of a Toyota Auris and includes a baseline configuration with a seat-back angle of 25°.

Fig. 1. Open-source seat model [6] and open-source vehicle model [5].

Assessment criteria

Prior to and after HBM positioning, the quality of the FE mesh was evaluated to ensure numerical stability and to identify potential element distortions introduced during the positioning procedure. Mesh quality metrics quantify the deviation of element geometry from an ideal reference configuration and are commonly used to detect distorted or degenerated elements that may reduce numerical accuracy or lead to instability in explicit FE simulations [7-8].

For shell elements, the evaluated metrics included aspect ratio, skewness, warping, taper, minimum element height, Jacobian determinant, minimum and maximum edge length, mesh distortion, and minimum and maximum internal angles for both quadrilateral and triangular elements. The aspect ratio is the ratio of the longest to the shortest element dimension and indicates element elongation. Skewness and taper quantify deviations from the ideal element shape, while warping describes the degree to which the nodes of a quadrilateral shell element deviate from a single plane. The Jacobian determinant characterises the transformation between the element’s local coordinate system and its physical geometry; values approaching zero indicate severe distortion or potential element inversion. The minimum element height and edge length metrics were evaluated to detect excessively small elements that could negatively affect the stability of the time step in explicit simulations.

For solid elements, the mesh quality evaluation included aspect ratio, element face warpage, minimum edge length, and element collapse indicators that describe potential degeneration of the element geometry and loss of element volume. Such distortions may lead to inaccurate strain and stress predictions or solver instabilities [7].

The evaluation of these metrics enabled verification that the mesh quality remained within commonly accepted limits for explicit crash simulations both before and after HBM positioning.

Mesh quality criteria were evaluated according to the element quality indicators implemented in the pre-processing software ANSA [9], which are widely used in crashworthiness FE modelling.

TABLE II
Quality criteria

Region	Mesh Quality Indicators	Recommended Limit
Shell elements	Aspect Ratio	<5
	Skewness	<60º
	Warping	<15º
	Taper	<0.5
	Jacobian	>0.7
	Mesh distortion	<0.6
	Minimum angle (quadrilaterals)	>45°
	Maximum angle (quadrilaterals)	<135°
	Minimum angle (triangles)	>20°
	Maximum angle (triangles)	<120°
Solid elements	Aspect ratio	<5
	Warping	<15º
	Collapse	0.2

The biomechanical injury metrics shown in Table III were used to assess the sensitivity of injury parameters to different positioning methods and seat compression. Injury metrics obtained with the different positioning methods were normalised to the reference configuration (Euro NCAP Capping Limits 2026). The risk of rib fractures has been set to 50% for three ages (25-year-old (yo), 45yo and 60yo) [10-11].

TABLE III

Region	Injury Metric	Euro NCAP Capping Limits 2026
Head	HIC [-]	700
	HIC - P (AIS2+)	31.3%
	HIC - P (AIS3+)	11.2%
	DAMAGE [-]	0.47
	DAMAGE – P (AIS2+)	65.6%
Neck	Peak Force [kN]	3.3
	Peak extension moment (My) [N*m]	57
Chest	Risk of Rib Fracture 25yo – P(AIS3+) (3+ broken ribs) [%]*	50%
	Risk of Rib Fracture 45yo – P(AIS3+) (3+ broken ribs) [%]*	50%
	Risk of Rib Fracture 65yo – P(AIS3+) (3+ broken ribs) [%]*	50%
Femur	Left/Right Femur peak axial force (Compression) [kN]	9.4
	Left/Right Femur peak bending moment [N*m]	440
Tibia	Left/Right Upper Tibia peak axial force [kN]	8.0
	Left/Right Upper Tibia peak bending moment [N*m]	320
	Left/Right Lower Tibia peak axial force [kN]	8.0
	Left/Right Lower Tibia peak bending moment [N*m]	320

* [10-11]

III. RESULTS

In total, 12 frontal impact simulations were conducted using three HBMs and four positioning methods. For each HBM, mesh quality criteria were evaluated before and after the positioning procedure in order to assess the influence of the positioning approach on mesh distortion. Furthermore, the effect of the positioning method on predicted injury metrics was analysed for each HBM individually.

Mesh Quality After Positioning

Finite element mesh quality deviations from the default (initial) posture were evaluated across all positioning methods and HBMs. Eleven mesh quality metrics were evaluated: aspect ratio, element skewness, warping, taper, Jacobian determinant, minimum element length, and minimum/maximum angles for both quadrilateral and triangular elements.

The following table shows the number of elements that fail the selected criteria in both the default posture of the HBM and the chosen positioning methods. Additional details can be found in Appendix D.

TABLE IV

NUMBER | PERCENTAGE OF FAILING ELEMENTS

METHOD	THUMS v4.1		THUMS v6.1		VIVA+ v2.0.1	
DEFAULT POSTURE	55524	2.90%	55560	2.90%	96971	12.41%
A/B	55790	2.91%	55747	2.91%	98317	12.59%
C	58946	3.08%	59123	3.09%	104968	13.44%
D	60544	3.16%	61126	3.19%	104720	13.41%

Data obtained using ANSA v25.1.2 Mesh Quality Inspector

Even from the default posture, HBMs had several failing elements. The THUMS models had 2.9% of elements failing the quality criteria, while VIVA+ had 12.41%. However, the number of failing elements remained consistent across the different positioning methods. Fig. 2 shows the mesh quality degradation from the default posture of the HBM per positioning method.

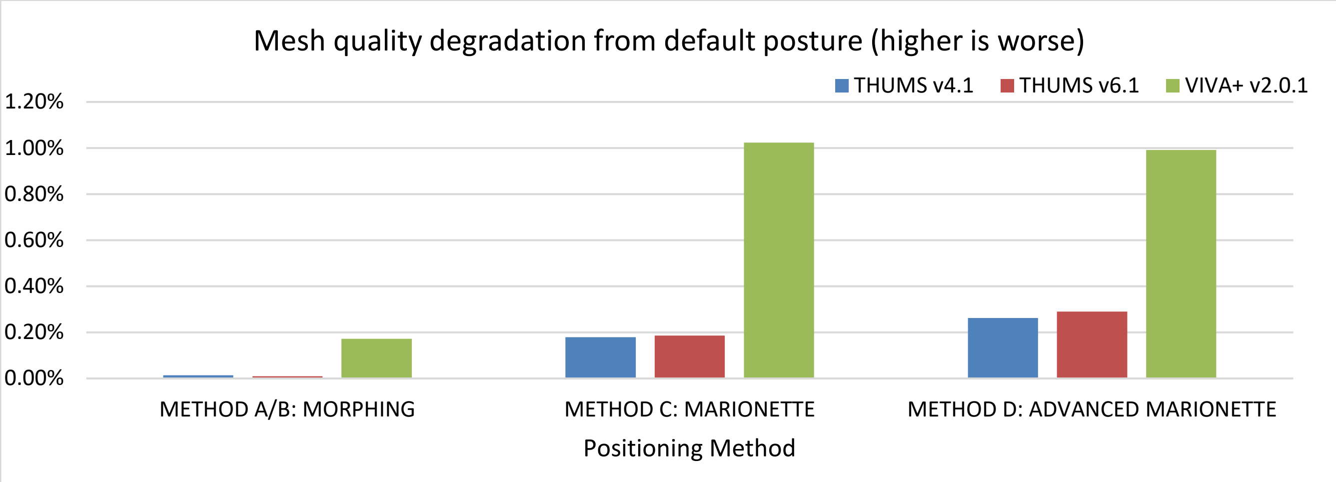

Fig. 2: Mesh quality degradation from the default posture of the HBM per positioning method.

Results show that total mesh quality degradation was below 1% in most cases, with VIVA+ in Method C being the only exception at 1.02%, indicating a small deviation from the initial values across the three HBM positioning methods.

Fig. 3 and Fig. 4 show the number of additional shell and solid elements that fail the criteria compared to the default posture after the HBM positioning procedure.

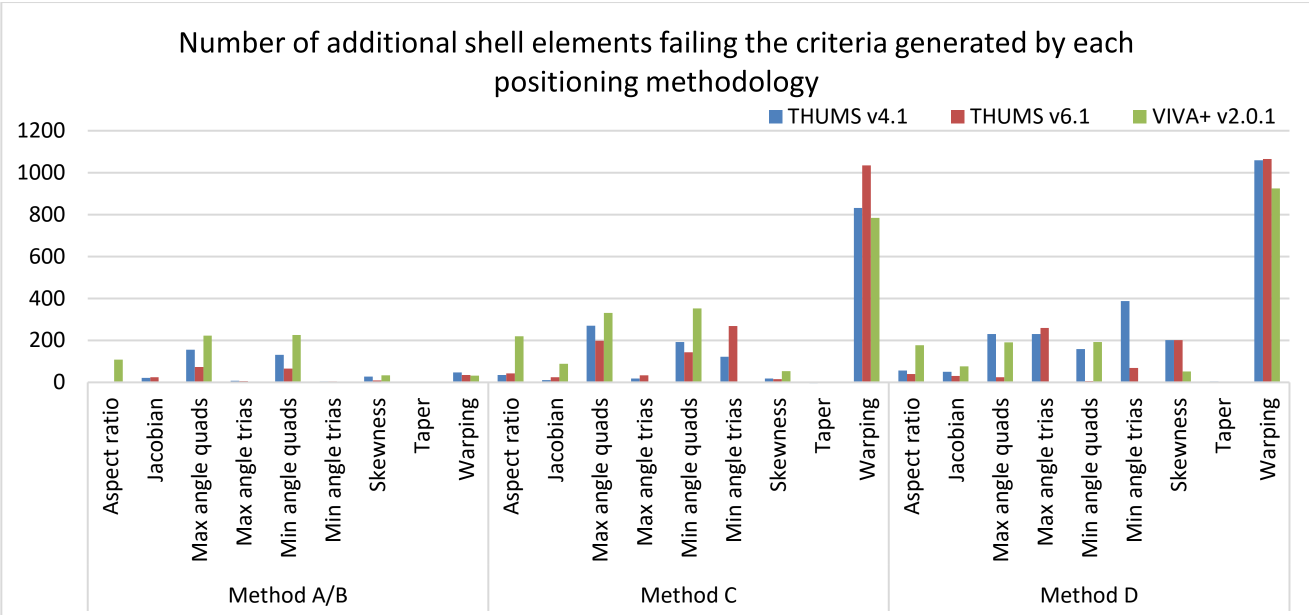

Fig. 3: Number of additional shell elements failing the criteria generated by each positioning methodology

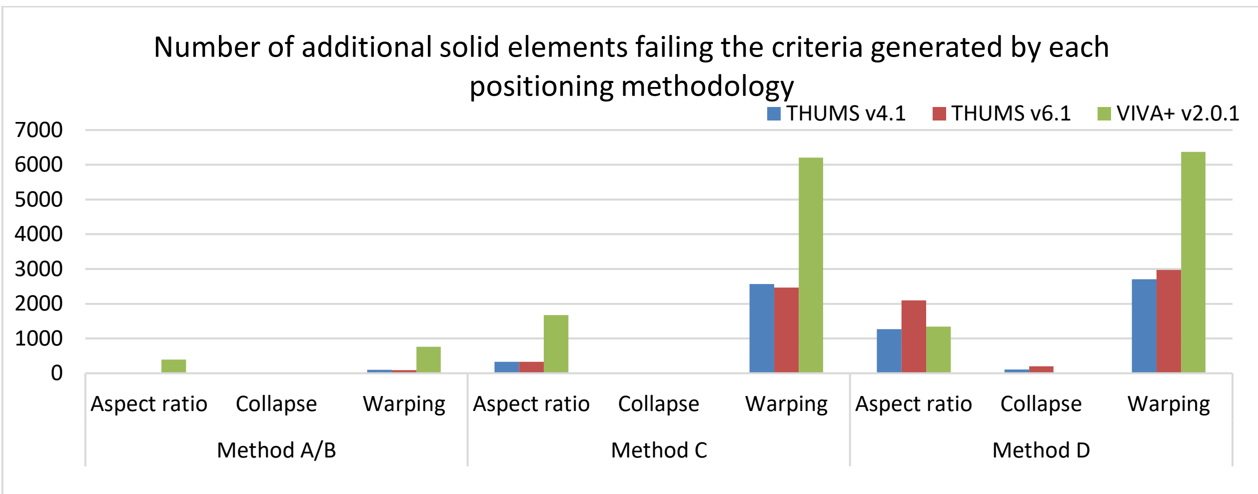

Fig. 4: Number of additional solid elements failing the criteria generated by each positioning methodology

Results show that morphing methodologies (Methods A and B) can keep the quality criteria quite close to the original default one for each simulation model. Simulation-based methods, however, tend to generate more failing elements due to the physical interactions that occur in simulation. Across all analysed metrics, Warping has been shown to be the most affected parameter in all scenarios and for all HBMs. Nonetheless, the number of shell elements that do not pass the criteria after positioning is less than the number of solid elements that fail. This might be because the three HBMs have more solid elements than shell elements (THUMS v4.1/v6.1 have around 1.92M elements, 450K shell and 1.47M solid; and VIVA+ v2.0.1 have 781K elements, 246K shell and 535K solid).

A cross-model comparison showed differences in sensitivity to positioning-dependent mesh degradation. VIVA+ M50 v2.0.1 consistently exhibited the highest number of element degradation across all methods, while being the model with the lowest number of elements (781K elements vs 1.92M elements for THUMS). THUMS v4.1 and v6.1 AM50 showed similar behaviour across all positioning methodologies.

Kinematic Evaluation

To assess the influence of positioning methodology on occupant kinematics, the trajectories of key anatomical landmarks were tracked throughout the simulation. Nine landmarks were selected for analysis: head centre of gravity (Head CoG), C1, C7, T8, T12, L5, acetabulum, knee, and ankle. Initial coordinate measurements confirmed that all positioning methods yielded identical starting positions for these landmarks, establishing a consistent baseline across all configurations with variations of less than 5 mm. Trajectory analysis revealed that the kinematics of the HBMs were nearly identical regardless of the positioning method employed, with negligible differences observed in the final postures of the landmarks following the crash event during the loading phase (Fig. 5).

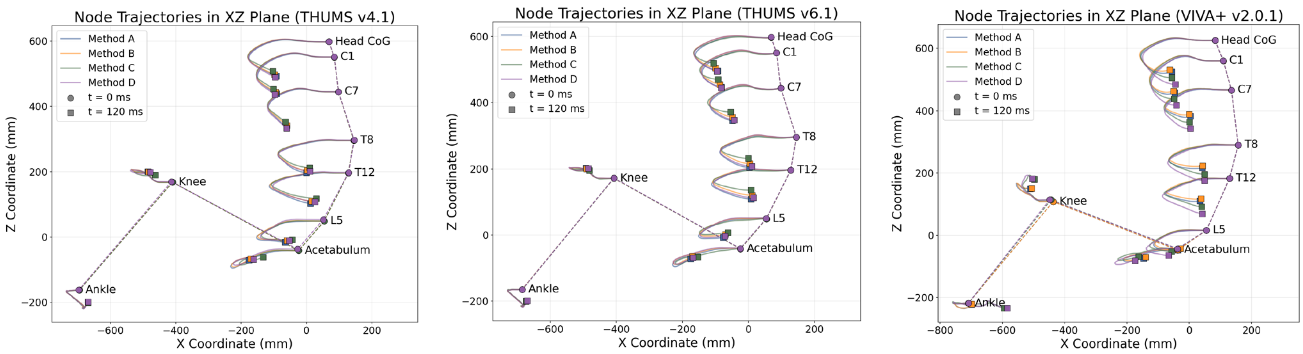

Fig. 5: Trajectories of HBMs' landmarks at the beginning of the crash simulation (t = 0ms) and at the end of the crash simulation (t = 120ms)

Influence of Positioning on Injury Metrics

Biomechanical injury prediction metrics presented in Table III were evaluated to assess the sensitivity of injury parameters to different positioning methods and seat-compression states across all three HBMs.

Head and Neck Response

Head injury predictions showed variability across positioning methods and surrogate models (Fig. 6). For HIC, THUMS v4.1 exhibited the widest method-to-method variation, ranging from 51.9% of the injury limit (*Method D*) to 102.8% (*Method B*). In contrast, THUMS v6.1 showed more stable HIC values (43.7–55.3% of injury limit), while VIVA+ demonstrated minimal method sensitivity (56.2–56.9% of injury limit, CV < 1%). Method variability for DAMAGE was more consistent across surrogates (CV: 6–11%). Notably, no consistent method ranking emerged across the two head injury metrics, with *Method B* producing the highest HIC but near-average DAMAGE values.

Fig. *7* shows peak axial force, which demonstrated stability across all methods and surrogates (overall CV < 2%). All three surrogates produced nearly identical force predictions for any given method, with maximum inter-surrogate variation not exceeding 3 percentage points. In contrast, peak extension moment (My) showed extreme sensitivity to positioning method, with *Method B* consistently producing values 2–3 times higher than other methods across all surrogates (16.4–18.8% of injury limit for *Method B* vs 5.8–11.7% for other methods).

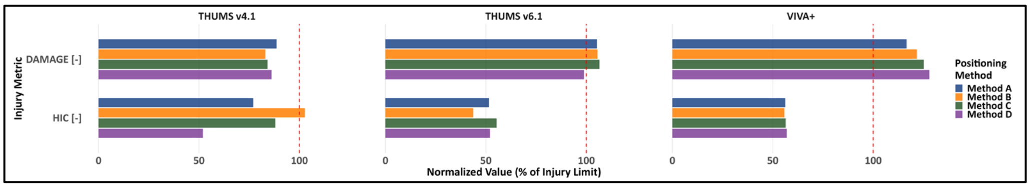

Fig. 6. Head injury metrics by positioning method and surrogate model. Methods: *A* (dark blue), *B* (orange), *C* (dark green), *D* (purple). Red line: injury threshold.

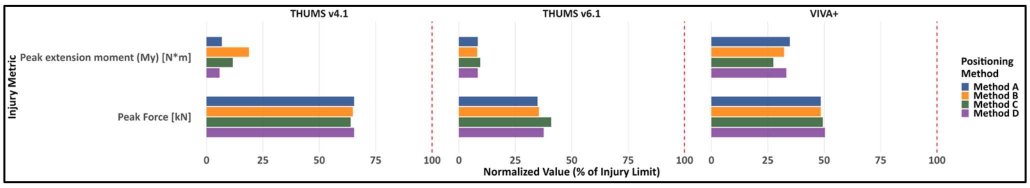

Fig. 7. Neck injury metrics by positioning method and surrogate model. Methods: A (dark blue), B (orange), C (dark green), D (purple). Red line: injury threshold.

Thoracic Response

Chest injury predictions showed different variations between methods with regard to age (Fig. 8). For 25yo occupants, rib fracture risk remained low across all methods and surrogates (1.2–2.9% of injury limit). *Method C* consistently produced the lowest fracture risk across all age groups and surrogates. As occupant age increased to 45yo, fracture risk predictions increased to 14.0–21.5% of the injury limit. For 65yo occupants, fracture risk approached critical levels (64.8–73.0% of injury limit), with method-to-method variation decreasing in relative terms (CV: 5–7% vs 15–20% for younger age groups) as all methods converged toward high injury probability. Inter-surrogate variation increased with age, with THUMS v4.1 predicting approximately 5–8 percentage points higher fracture risk than other surrogates for elderly occupants.

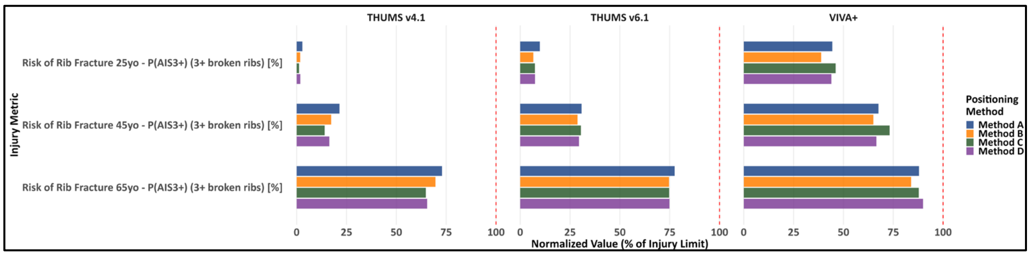

Fig. 8. Chest injury metrics by positioning method and surrogate model. Methods: *A* (dark blue), *B* (orange), *C* (dark green), *D* (purple). Red line: 50% probability of rib fracture.

Lower Extremity Response

Femur injury metrics showed distinct method variability patterns for axial and bending loading metrics (Fig. 9). Left femur peak axial forces demonstrated low method sensitivity (CV: 3–5%), with minimal variation between Methods *A*, *B*, and *D*, while *Method C* produced reduced values. Left femur peak bending moments exhibited greater method variability (CV: 12–18%), with *Method C* distinctively producing values 15–20% higher than other methods across all surrogates. Right femur axial forces demonstrated moderate method variability (CV: 8–12%), and right femur bending moments showed high method variability (CV: 12–18%) that was nearly identical to the left side.

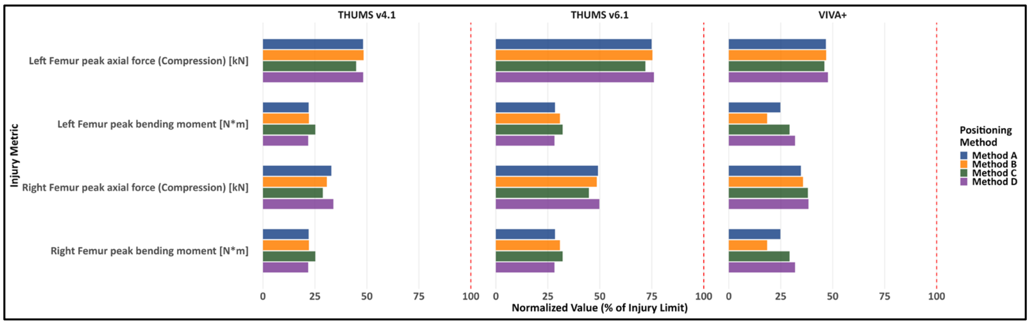

Fig. 9. Femur injury metrics by positioning method and surrogate model. Methods: *A* (dark blue), *B* (orange), *C* (dark green), *D* (purple). Red line: injury threshold.

Tibia injury metrics showed the greatest complexity, with eight different loading metrics demonstrating varied method sensitivities (Fig. 10). Upper tibia axial forces demonstrated high method variability (CV: 15–25%), with *Method C* consistently producing the highest values and *Method B* the lowest across all surrogates. Upper tibia bending moments showed moderate method variability (CV: 10–18%). Bilateral comparisons revealed that right upper tibia forces exhibited lower method variability (CV: 8–12%) than left-side forces (CV: 15–25%). Lower tibia axial forces maintained high method variability (CV: 12–20%). Lower tibia bending moments demonstrated the highest method variability in the tibia region (CV: 15–22%).

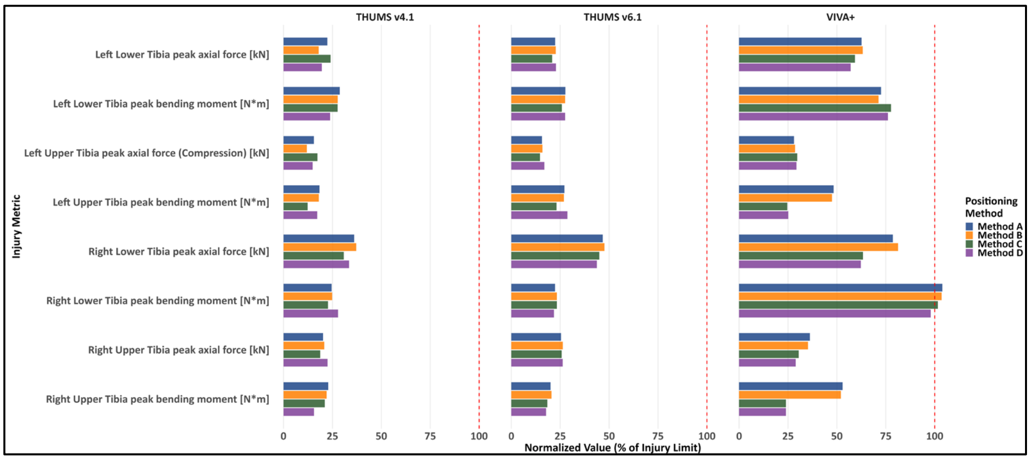

Fig. 10. Tibia injury metrics by positioning method and surrogate model. Methods: A (dark blue), B (orange), C (dark green), D (purple). Red line: injury threshold.

Method variability across all injury metrics was quantified using the coefficient of variation (CV) calculated within each surrogate model (Fig. 11). Peak extension moment demonstrated the highest method sensitivity (CV: 45–68% across surrogates), while peak axial force showed negligible variability (CV < 2%). Method–surrogate interactions were evident in several metrics, shown by divergent bar heights across the three models. HIC exhibited strong interaction effects, with THUMS v4.1 showing high method variability (CV: 27%), while THUMS v6.1 and VIVA+ showed minimal variability (CV < 10%). Conversely, chest rib fracture risk and femur bending moments displayed consistent CV values across all surrogates (bar heights similar), indicating method effects independent of computational model choice. Of 19 metrics analysed, eight demonstrated substantial method–surrogate interactions (CV differences > 10% between surrogates), while 11 showed consistent method sensitivity across models. Tibia metrics exhibited the most complex patterns, with multiple interactions, particularly for bending moments, where method rankings changed by surrogate. These findings indicate that the effectiveness of positioning methods is model-dependent for approximately 40% of injury metrics, with implications for the generalisability of positioning optimisation strategies.

Complete simulation results are provided in Appendix A.

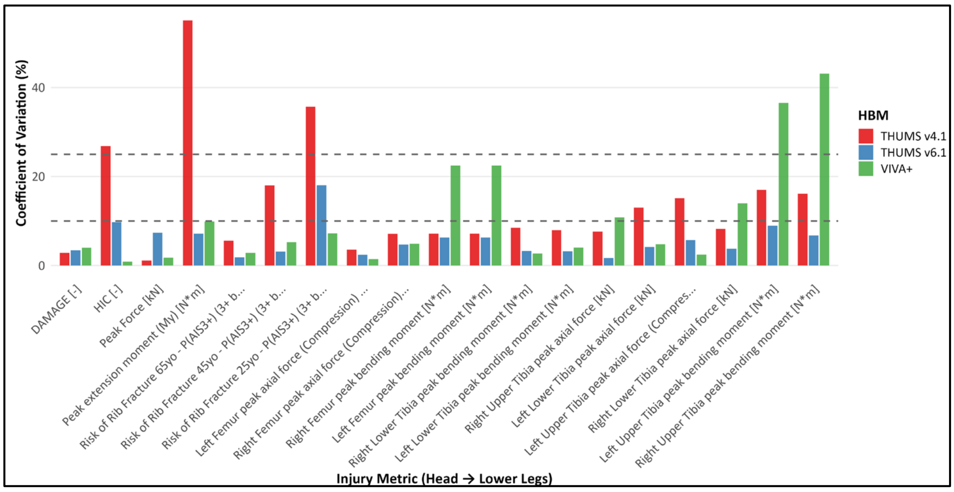

Fig. 11. Coefficient of variation (CV) of injury metrics across the four positioning methods, shown separately for each surrogate model (Red: THUMS v4.1; Blue: THUMS v6.1; Green: VIVA+). Dashed lines indicate CV thresholds at 10% and 25%.

IV. DISCUSSION

Mesh quality

Previous studies have demonstrated that injury predictions using FE HBMs are sensitive to subject-specific characteristics and modelling assumptions [12-13]. In parallel, several approaches have been proposed to address the challenges of repositioning HBMs while maintaining mesh quality [1-2]. However, the influence of the positioning methodology itself on variability in injury prediction remains largely unexplored.

Mesh verification procedures similar to those used in the development of established HBMs were applied in this study. Previous HBM developments include verification of element distortion, Jacobian determinant and aspect ratio to ensure numerical robustness [14]. The minimal mesh quality degradation observed across all positioning methods (<1% in most cases, up to 1.02% for VIVA+ Method C) demonstrates that contemporary HBMs possess sufficient geometric and material definition to withstand repositioning without substantial element deterioration. These findings align with [15], who reported that postural adjustment times of 100 ms using THUMS v4.1 maintained acceptable element quality while achieving target postures with mean joint angular velocities up to 367 deg/s. However, the present study reveals that VIVA+ M50 v2.0.1, despite having substantially fewer elements (781,000 vs 1,920,000 for THUMS models), exhibited the highest baseline failing-element count (12.41%) and the greatest degradation across all methods. This suggests that preserving element quality during positioning depends not only on mesh resolution but also on the underlying model architecture, material property definitions, and the geometric complexity of soft tissue regions.

The observation that morphing-based approaches (Methods A and B) preserved mesh quality more effectively than simulation-based methods (Methods C and D) was anticipated, given their fundamentally different deformation mechanisms. Morphing enforces geometric conformity through prescribed nodal displacements while maintaining internal topology, whereas simulation-based methods permit mutual deformation through contact interactions that can induce localised element distortion. The warping parameter emerged as the most affected quality metric across all scenarios. The higher proportion of failing solid elements relative to shell elements likely reflects the greater geometric constraints imposed on volumetric tissue representations, particularly in regions with complex three-dimensional curvature such as the abdominal region, the gluteal region and the thoracic cavity.

Kinematic response

The near-identical gross kinematics observed during the loading phase across all positioning methods and HBMs is an important finding that initially suggests positioning methodology has negligible influence on occupant response. All methods achieved identical target landmark positions and produced indistinguishable trajectories for the 9 anatomical landmarks tracked from impact initiation through 120 ms. This kinematic equivalence is consistent with [16], which reported maximum deviations of 10 mm at the knee and 5° in head angle when positioning three different HBMs (two finite-element, one multibody) to a common target posture using simulation-based landmark positioning. However, the present study's finding of substantial variability in injury metrics despite kinematic similarity suggests that local tissue-level deformation states, rather than gross occupant motion, govern injury prediction outcomes in HBM simulations.

Injury metrics

This study demonstrates that positioning methodology introduces substantial variability in injury predictions, with the magnitude and pattern of this variability being highly metric-specific and model-dependent. Analysis of 19 injury metrics across four positioning methods and three surrogate models revealed a coefficient of variation ranging from less than 2% to 68%, indicating that positioning sensitivity is not uniform across injury metrics but rather depends on the specific body region being evaluated (Fig. 11). Neck peak extension moment showed extreme positioning sensitivity (CV: 45–68%), with Method B yielding values 2–3 times higher than those of other methods (16.4–18.8% vs 5.8–11.7% within chosen limits). This suggests morphing-based positioning with pre-simulation seat deformation creates cervical spine loading states that amplify extension moments. HIC demonstrated model-dependent sensitivity: THUMS v4.1 showed 27% CV (range: 51.9–102.8% of limits, spanning regulatory thresholds) versus <10% CV for THUMS v6.1 and VIVA+.

Rib fracture risk showed an inverse relationship between positioning sensitivity and age: 25-year-olds exhibited CV of 15–20% (risk: 1.2–2.9% of limits) while 65-year-olds showed CV of 5–7% but approached critical levels (64.8–73.0% of limits). This convergence suggests that elderly tissue failure thresholds are reached across a broader range of loading conditions. Method C consistently produced the lowest fracture risk, possibly due to gravity-based settling creating more physiologically representative thoracic geometry.

THUMS v4.1 predicted a 5–8 percentage-point higher risk of elderly rib fracture than other models, consistent with material property differences between versions. Nevertheless, all surrogates approached 70% of the limits for elderly occupants.

Femur axial force showed low positioning sensitivity (CV: 3–5%), whereas femur bending moments and especially tibia metrics exhibited substantially greater variability (CV: 8–25%), indicating that positioning methodology and lower-extremity alignment strongly influence lower-limb injury responses, consistent with previous findings on anthropometric and posture effects.

From a practical standpoint, the findings inform resource allocation decisions. Computational requirements varied substantially across methods, with *Method A* requiring minimal set-up (2–4 hours engineering time, no pre-simulation) and total simulation times of 7–12 hours using 96 CPUs, while Methods *C* and *D* required extended pre-processing (5.5–6.5 hours pre-simulation) with total times reaching 16–18 hours for THUMS v6.1. Engineering complexity escalated from simple morphing operations (Methods *A* and *B*, categorised as "Easy") to medium-complexity marionette approaches (Method C) and advanced marionette techniques (Method D, categorised as "Hard" and requiring an additional 1–2 hours of pre-simulation set-up expertise).

Limitations

Several limitations must be acknowledged. First, only three 50th percentile male HBMs were evaluated in frontal impacts. Extension to different anthropometries and alternative impact modes (side, rear, oblique) is needed to establish generalizability across real-world crash scenarios. Second, a single seat model (Toyota Auris) was employed. Real-world seats vary substantially in foam stiffness, geometry, and bolster design, which may interact with positioning methodology to alter the sensitivity of injury metrics. Evaluation across diverse seat designs would clarify seat-geometry dependencies. Third, injury metrics were limited to Euro NCAP 2026 protocols. Advanced indicators, including tissue strain predictions or organ-level criteria, were not analysed. Positioning sensitivity of these metrics remains unknown. Fourth, mesh quality assessment used geometric criteria (aspect ratio, skewness, warping) as computational proxies but did not quantify anatomical fidelity. Integration of anatomical accuracy metrics, organ volume preservation, tissue thickness consistency, and skeletal alignment conformity with medical imaging would provide a more comprehensive evaluation. Fifth, no experimental validation was performed. While individual components have been validated independently, the specific HBM configurations in this position lack direct experimental validation. Comparison with PMHS data using matched postures or volunteer kinematics would substantiate the observed effects. Finally, the 120 ms duration captures primary loading but excludes rebound and secondary contacts that may exhibit different positioning sensitivities. An extended analysis using complete kinematics would provide a comprehensive understanding of the crash sequence.

Future Work

Despite similar mesh quality and kinematics across the four positioning methods in the three HBMs, notable differences in injury metrics arose due to different soft-tissue deformation at the occupant-seat interface during positioning. Morphing approaches (Methods A and B) enforce geometric conformity while preserving internal tissue topology, whereas simulation methods (Methods C and D) allow mutual deformation through physical interaction. These initial stress and strain differences influence load path development and injury prediction. It remains unclear which method better replicates real occupant conditions, affecting biofidelic injury estimates. Future research with more scenarios and HBMs could clarify if metric variances are scenario-specific or generalizable, and whether they reflect realistic occupant diversity or computational artifacts.

V. CONCLUSION

This study evaluated the influence of occupant positioning methodology on injury prediction and mesh quality in FE HBM simulations. Four positioning methods were compared across three HBMs (THUMS v4.1 AM50, THUMS v6.1 AM50, and VIVA+ M50 v2.0.1) under frontal impact loading conditions. The following conclusions can be drawn.

- Mesh quality degradation after positioning was minimal (<1% additional failing elements), with morphing-based methods preserving quality best.
- Occupant kinematics were nearly identical across methods despite different positioning approaches.
- Injury metrics showed strong, metric-specific sensitivity to positioning (CV: <2%–68%), despite similar kinematics.
- Axial force metrics were robust to positioning, while bending and extension moments were highly sensitive.
- Lower-extremity injury metrics, especially tibia responses, showed the greatest variability and complexity.
- Positioning effectiveness was model-dependent, preventing universal best-practice recommendations.
- Differences in soft tissue pre-stress between morphing and simulation-based methods may explain injury metric variability.
- Computational cost varied widely, with Method A being the fastest and least complex, and Methods C/D requiring the highest processing time.

This investigation reveals that while HBM positioning methodologies produce equivalent kinematics and acceptable mesh quality, injury prediction outcomes exhibit non-negligible method-specific and model-dependent variations. The development of biofidelic positioning protocols, validated against measurements of real human tissue deformation and contact pressure distributions during sitting, represents a critical frontier in computational injury biomechanics that will enhance the accuracy and reliability of HBMs for virtual testing in automotive safety research.

AI Use Disclosure: a generative artificial intelligence tool (an internal, private company tool, AIDA) was used to support language editing and/or manuscript organisation. All scientific content, interpretations, and conclusions were developed, reviewed, and validated by the authors, who take full responsibility for the accuracy and integrity of the work.

VI. REFERENCES

[1] Beillas, P., Petit, P., Kleiven, S. (2015) Specifications of a Software Framework to Position and Personalise Human Body Models. *Proceedings of the IRCOBI Conference*, 2015, Lyon, France.

[2] Tang, J., Zhou, Q., Shen, W., Chen, W., Tan, P. (2023) Can we reposition finite element human body model like dummies? *Frontiers in Bioengineering and Biotechnology*, **11**: p. 1176818. doi: 10.3389/fbioe.2023.1176818.

[3] Chen, S. and Li, X. (2025) A Laplacian-based framework for finite element human body model positioning. *Frontiers in Bioengineering and Biotechnology*, **13**: p. 1599010. doi: 10.3389/fbioe.2025.1599010.

[4] Zhang ,K., *et al.* (2017) An automated method to morph finite element whole-body human models with a wide range of stature and body shape for both men and women. *Journal of Biomechanics*, *60*: pp. 253–260. doi: 10.1016/j.jbiomech.2017.06.015.

[5] Singh, H., Ganesan, V., Davies, J., Paramasuwom, M., Gradischnig, L. (2018) Vehicle interior and restraints modeling development of full vehicle finite element model including vehicle interior and occupant restraints systems for occupant safety analysis using THOR dummies. National Highway Traffic Safety Administration, Washington, D.C., DOT HS 812 545.

[6] VIRTUAL Project, https://projectvirtual.eu.

[7] Belytschko, T. (2014) *Nonlinear Finite Elements for Continua and Structures*, 1st ed. In: New York Academy of Sciences Series. Newark: John Wiley & Sons, Incorporated.

[8] Zienkiewicz, O. C., Taylor, R. L., Govindjee, S. (2025) *The finite element method: its basis and fundamentals*, 8th edition. London: Butterworth-Heinemann, 2025.

[9] *ANSA User's Guide – Mesh Quality Criteria.* BETA CAE Systems.

[10] Larsson, K.-J., Blennow, A., Iraeus, J., Pipkorn, B., Lubbe, N. (2021) Rib Cortical Bone Fracture Risk as a Function of Age and Rib Strain: Updated Injury Prediction Using Finite Element Human Body Models. *Frontiers in Bioengineering and Biotechnology*, **9**: p. 677768,. doi: 10.3389/fbioe.2021.677768.

[11] Forman, J., Kulkarni, S., Perez-Rapela, D. (2022) A Method for Thoracic Injury Risk Function Development for Human Body Models. *Proceedings of the IRCOBI Conference*, 2022, Porto, Portugal.

[12] Iraeus, J., *et al.* (2019) Detailed subject-specific FE rib modeling for fracture prediction. *Traffic Injury Prevention*, **20**(sup2): pp. S88–S95,. doi: 10.1080/15389588.2019.1665649.

[13] Untaroiu, C. D., Yue, N., Shin, J. (2013) A Finite Element Model of the Lower Limb for Simulating Automotive Impacts. *Annals of Biomedical Engineering*, **41**(3): pp. 513–526. doi: 10.1007/s10439-012-0687-0.

[14] John, J., Klug, C., Kranjec, M., Svenning, E., Iraeus, J. (2022) Hello, world! VIVA+: A human body model lineup to evaluate sex-differences in crash protection. *Frontiers in Bioengineering and Biotechnology*, **10**: p. 918904. doi: 10.3389/fbioe.2022.918904.

[15] C. Costa, R. Herriott, and Y. Huang, "Effect of Postural Adjustment Methods on Mesh Quality and Simulation Time of Human Body Models," in *Proc. IRCOBI Conf.*, IRC-21-XX, 2021.

[16] Klein, C., González-García, M., Weber, J., Bosma, F., Lancashire, R., Breitfuss, D., Kirschbichler, S., & Leitgeb, W. (2021). A Method for Reproducible Landmark-based Positioning of Multibody and Finite Element Human Models. IRC-21-53, IRCOBI Conference 2021.

[17] Leledakis, A. "Heterogeneity in Car Occupant Safety – Using Numerical Simulations to Improve Understanding of Real-World Safety Factors," PhD thesis, Chalmers Univ. Technol., Gothenburg, Sweden, 2022.

[18] Leledakis, A., Lindman, M., Östh, J., Wågström, L., Davidsson, J., and Jakobsson, L., "The Influence of Car Passenger Sitting Postures in Intersection Crashes," in *Proc. IRCOBI Conf.*, IRC-21-XX, 2021.

VII. APPENDIX

Appendix A: Simulation results

TABLE A1
THUMS V4.1 AM50 SIMULATION RESULTS

Region	***Injury Metric***	***THUMS V4.1 AM50***			
		Method_A	***Method_B***	***Method_C***	***Method_D***
Head	HIC [-]	539,4	719,5	616,3	363,6
	HIC - P (AIS2+)	21,3%	32,5%	26,2%	10,4%
	HIC - P (AIS3+)	5,8%	11,9%	8,2%	1,8%
	DAMAGE [-]	0,42	0,39	0,40	0,40
	DAMAGE – P(AIS2+)	49,4%	41,5%	43,0%	45,8%
Neck	Peak Force [kN]	2,16	2,14	2,11	2,16
	Peak extension moment (My) [N*m]	3,89	10,72	6,66	3,3
Chest	Risk of Rib Fracture 25yo – P(AIS3+) (3+ broken ribs) [%]	1,4%	0,9%	0,6%	0,9%
	Risk of Rib Fracture 45yo – P(AIS3+) (3+ broken ribs) [%]	10,7%	8,7%	7,0%	8,2%
	Risk of Rib Fracture 65yo – P(AIS3+) (3+ broken ribs) [%]	36,5%	34,8%	32,4%	32,7%
Femur	Left Femur peak axial force (Compression) [kN]	4,38	4,40	4,08	4,38
	Left Femur peak bending moment [N*m]	96,73	97,18	110,85	95,73
	Right Femur peak axial force (Compression) [kN]	2,99	2,80	2,62	3,08
	Right Femur peak bending moment [N*m]	96,73	97,18	110,85	95,73
Tibia	Left Upper Tibia peak axial force [kN]	1,24	0,95	1,39	1,19
	Left Upper Tibia peak bending moment [N*m]	58,91	57,75	39,54	55,07
	Right Upper Tibia peak axial force [kN]	1,62	1,67	1,50	1,80
	Right Upper Tibia peak bending moment [N*m]	73,23	70,66	67,69	49,91
	Left Lower Tibia peak axial force [kN]	1,79	1,44	1,92	1,57
	Left Lower Tibia peak bending moment [N*m]	91,98	88,54	88,44	76,38
	Right Lower Tibia peak axial force [kN]	2,89	2,97	2,47	2,68
	Right Lower Tibia peak bending moment [N*m]	78,73	79,55	72,80	89,22

TABLE A2
THUMS V6.1 AM50 SIMULATION RESULTS

Region	***Injury Metric***	***THUMS V6.1 AM50***			
		Method_A	***Method_B***	***Method_C***	***Method_D***
Head	HIC [-]	360,9	305,7	387,1	364,5
	HIC – P (AIS2+)	10,2%	7,1%	11,8%	10,4%
	HIC – P (AIS3+)	1,7%	1,0%	2,2%	1,8%
	DAMAGE [-]	0,50	0,50	0,50	0,46
	DAMAGE – P(AIS2+)	72,7%	72,9%	74,2%	64,1%
Neck	Peak Force [kN]	1,15	1,17	1,35	1,24
	Peak extension moment (My) [N*m]	4,76	4,62	5,4	4,76
Chest	Risk of Rib Fracture 25yo – P(AIS3+) (3+ broken ribs) [%]	4,9%	3,3%	3,7%	3,7%
	Risk of Rib Fracture 45yo – P(AIS3+) (3+ broken ribs) [%]	15,4%	14,4%	15,2%	14,7%
	Risk of Rib Fracture 65yo – P(AIS3+) (3+ broken ribs) [%]	38,7%	37,3%	37,4%	37,4%
Femur	Left Femur peak axial force (Compression) [kN]	6,82	6,85	6,54	6,92
	Left Femur peak bending moment [N*m]	125,19	135,61	141,22	124,03

	Right Femur peak axial force (Compression) [kN]	4,47	4,42	4,07	4,53
	Right Femur peak bending moment [N*m]	125,19	135,61	141,22	124,03
Tibia	Left Upper Tibia peak axial force (Compression) [kN]	1,25	1,28	1,18	1,35
	Left Upper Tibia peak bending moment [N*m]	86,78	86,05	74,01	91,89
	Right Upper Tibia peak axial force [kN]	2,03	2,11	2,06	2,10
	Right Upper Tibia peak bending moment [N*m]	64,14	65,75	58,98	56,95
	Left Lower Tibia peak axial force [kN]	1,80	1,82	1,67	1,83
	Left Lower Tibia peak bending moment [N*m]	88,55	88,20	82,76	88,10
	Right Lower Tibia peak axial force [kN]	3,74	3,81	3,60	3,50
	Right Lower Tibia peak bending moment [N*m]	71,53	74,59	74,47	69,71

TABLE A3

VIVA M50 V2.0.1+ SIMULATION RESULTS

Region	***Injury Metric***	***VIVA+ 50M***			
		Method_A	***Method_B***	***Method_C***	***Method_D***
Head	HIC [-]	393,1	390,7	394,6	398,7
	HIC – P (AIS2+)	12,1%	12,0%	12,2%	12,5%
	HIC – P (AIS3+)	2,3%	2,2%	2,3%	2,4%
	DAMAGE [-]	0,55	0,57	0,59	0,60
	DAMAGE – P(AIS2+)	85,0%	89,3%	91,6%	93,2%
Neck	Peak Force [kN]	1,6	1,6	1,63	1,66
	Peak extension moment (My) [N*m]	19,83	18,36	15,67	18,95
Chest	Risk of Rib Fracture 25yo – P(AIS3+) (3+ broken ribs) [%]	22,2%	19,4%	23,1%	22,0%
	Risk of Rib Fracture 45yo – P(AIS3+) (3+ broken ribs) [%]	33,8%	32,5%	36,6%	33,3%
	Risk of Rib Fracture 65yo –P(AIS3+) (3+ broken ribs) [%]	43,9%	42,0%	43,9%	45,0%
Femur	Left Femur peak axial force (Compression) [kN]	4,25	4,27	4,19	4,34
	Left Femur peak bending moment [N*m]	109,23	81,22	128,72	140,21
	Right Femur peak axial force (Compression) [kN]	3,15	3,25	3,46	3,49
	Right Femur peak bending moment [N*m]	109,23	81,22	128,72	140,21
Tibia	Left Upper Tibia peak axial force (Compression) [kN]	2,25	2,29	2,38	2,34
	Left Upper Tibia peak bending moment [N*m]	154,70	152,02	78,85	80,35
	Right Upper Tibia peak axial force [kN]	2,90	2,82	2,44	2,32
	Right Upper Tibia peak bending moment [N*m]	169,28	166,61	76,63	76,65
	Left Lower Tibia peak axial force [kN]	5,01	5,06	4,74	4,57
	Left Lower Tibia peak bending moment [N*m]	232,18	228,04	248,58	243,54
	Right Lower Tibia peak axial force [kN]	6,29	6,50	5,07	4,98
	Right Lower Tibia peak bending moment [N*m]	332,42	331,47	325,17	313,47

Appendix B: Method Influence Heatmap

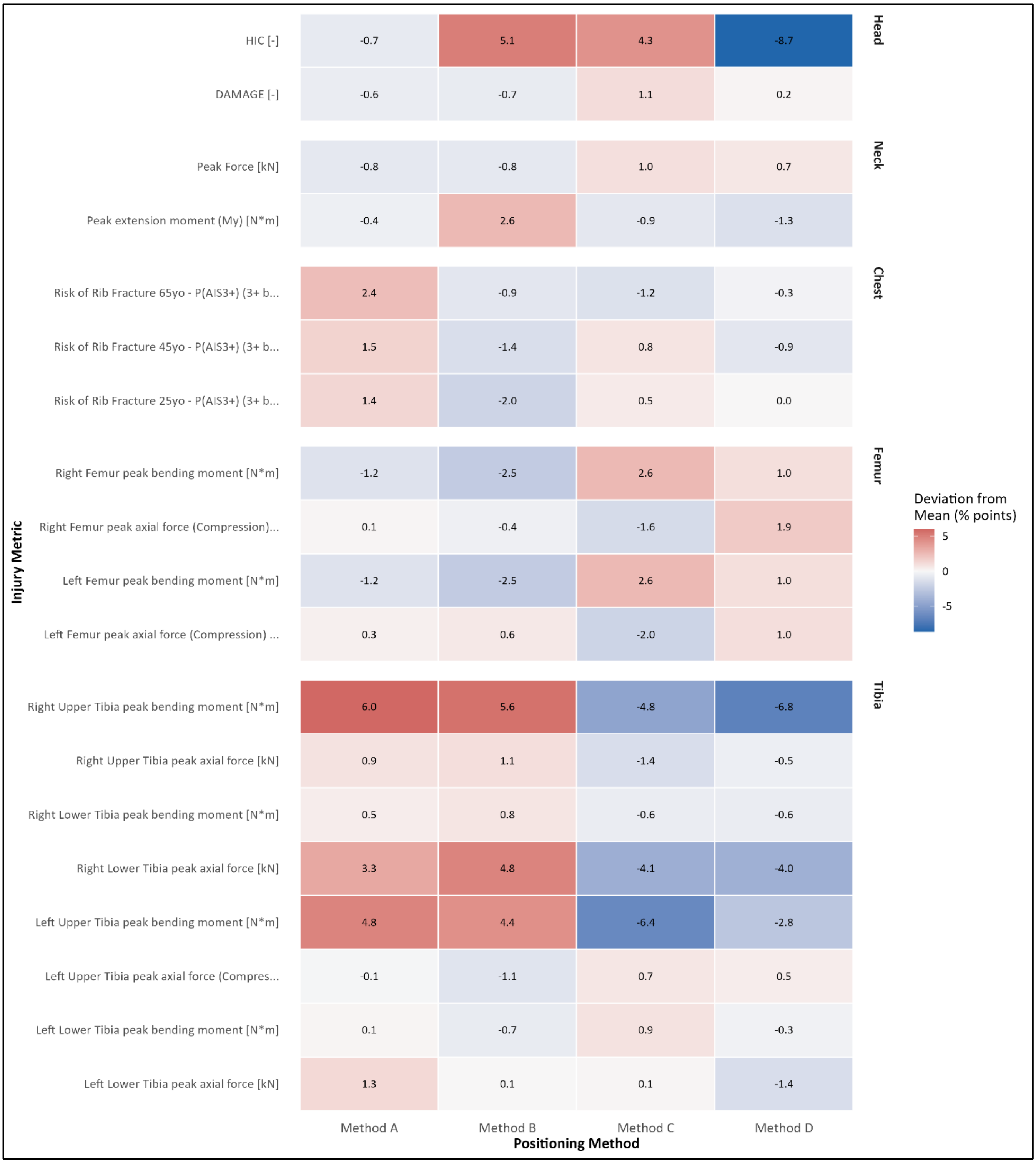

Fig. B1. Positioning method influence on injury metrics. Deviation from overall mean (averaged across all surrogate models) for each injury metric. Positive values (red) indicate methods producing above-average injury predictions; negative values (blue) indicate below-average predictions. Values shown in percentage points relative to injury limit.

Appendix C: Surrogate Influence Heatmap

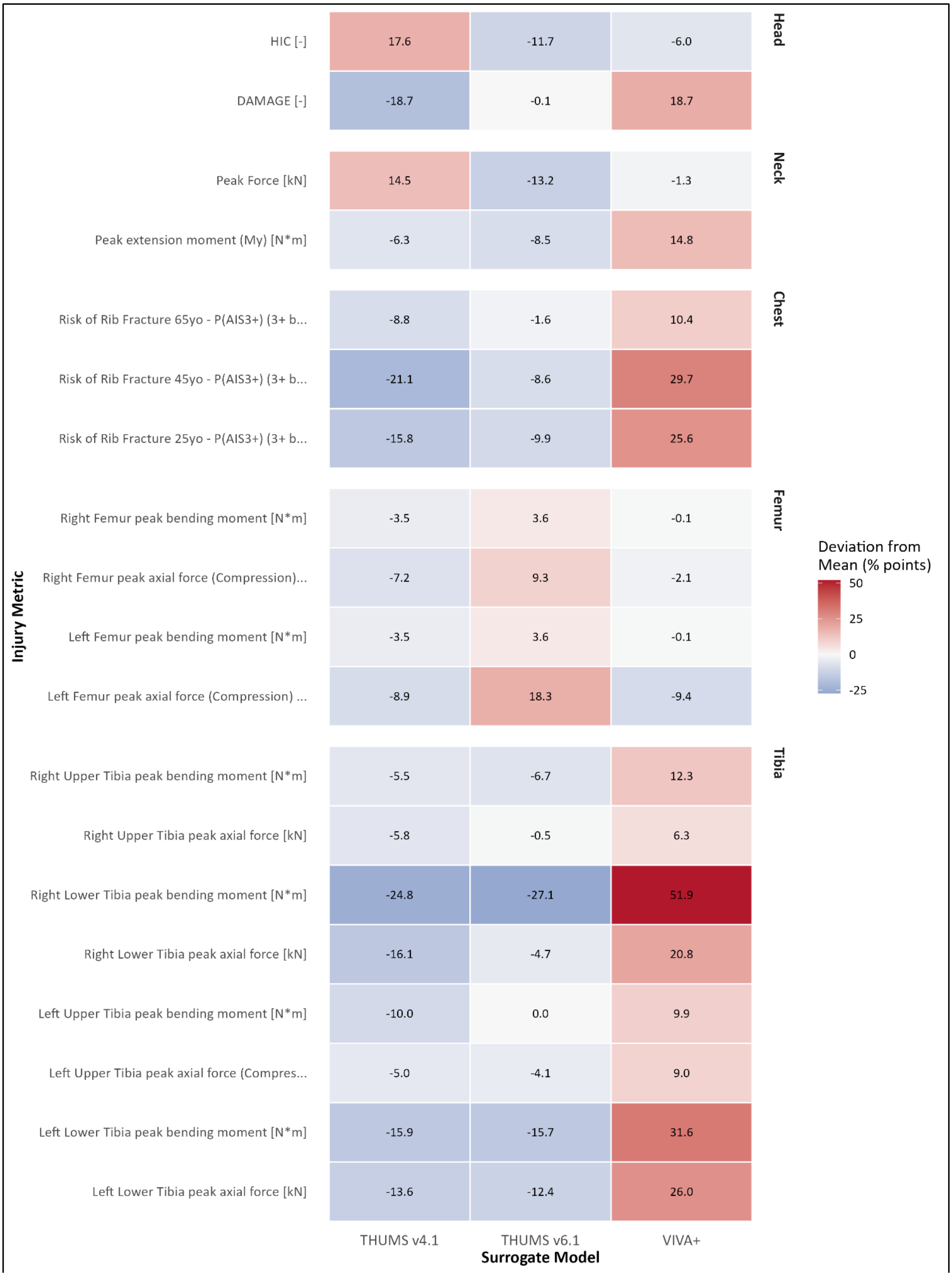

Fig. C1. Surrogate model influence on injury metrics. Deviation from overall mean (averaged across all positioning methods) for each injury metric. Positive values (red) indicate surrogates producing above-average injury predictions; negative values (blue) indicate below-average predictions. Values shown in percentage points relative to injury limit.

Appendix D: Body Region wise Quality

Type	Quality parameters		DEFAULT POSITION HBM			METHOD A/B: MORPHING			METHOD C: MARIONETTE			METHOD D: ADVANCED MARIONETTE		
			THUMS V41	THUMS V61	VIVA+ V201	THUMS V41	THUMS V61	VIVA+ V201	THUMS V41	THUMS V61	VIVA+ V201	THUMS V41	THUMS V61	VIVA+ V201
Shells	Aspect ratio	5	1250	1250	1578	1250	1250	1686	1285	1293	1798	1306	1290	1755
	Skewness	60	601	601	142	628	611	176	620	617	195	803	803	194
	Warping	15	12797	12817	9193	12845	12852	9225	13629	13851	9978	13856	13883	10118
	Taper	0,5	79	79	13	79	79	13	75	77	13	83	81	15
	Jacobian	0,7	6671	6669	3502	6693	6694	3502	6682	6694	3590	6721	6700	3579
	Min angle quads	45	3120	3120	4468	3252	3186	4694	3312	3264	4820	3279	3126	4660
	Max angle quads	135	4200	4202	5099	4356	4275	5322	4470	4401	5431	4430	4226	5290
	Min angle trias	20	1212	1212	14	1216	1216	14	1334	1481	14	1599	1281	14
	Max angle trias	120	276	276	11	283	282	11	294	310	10	506	536	11
Solids	Aspect ratio	5	6239	6239	30344	6249	6255	30734	6570	6568	32022	7504	8338	31684
	Warping	15	27163	27179	58595	27260	27266	59361	29727	29641	64802	29871	30148	64970
	Collapse	0,2	315	315	0	317	317	0	327	320	0	421	520	0
Totals	Total elements		1916046	1916206	781131	1916046	1916206	781131	1916046	1916206	781131	1916046	1916206	781131
	Total failing elements		55524	55560	96971	55790	55747	98317	58946	59123	104968	60544	61126	104720
	% Of failing elements		2,90%	2,90%	12,41%	2,91%	2,91%	12,59%	3,08%	3,09%	13,44%	3,16%	3,19%	13,41%

Appendix E: HBM model comparison

TABLE E1
HBM MODEL COMPARISON

Feature	*THUMS v4.1 / v6.1*	*VIVA+ M50 v2.0.1*
Total elements	~1.92M (450K shell + 1.47M solid)	~781K (246K shell + 535K solid)
Target element size	3–5 mm (documented)	Not specified
Joint element type at articulations	Tetrahedral flesh (ELFORM=13) for "easy remeshing"	Hexahedral (ELFORM=1) + kinematic joints
Knee joint	Deformable solid ligaments + sliding contacts	Discrete beam elements (1D springs)
Ankle/Elbow joints	Organic (bone-to-bone with ligaments)	Kinematic (revolute/spherical)
Thoracic spine joints	Deformable intervertebral discs (solid)	Zero-length 6DOF discrete beams
Skin-to-flesh connectivity	Shared nodes (direct coupling)	Membrane (ELFORM=9) + tiebreak contacts
Inter-muscle connectivity	Sliding contacts between flesh parts	Single adipose layer (MAT_OGDEN_RUBBER)
Model generation (50M)	Direct from male CT data	Morphed from 50F base model
Pre-positioning Jacobian failures	0 (abdomen)	272 elements (abdomen)

Appendix F: Vehicle model behavior across the four methods

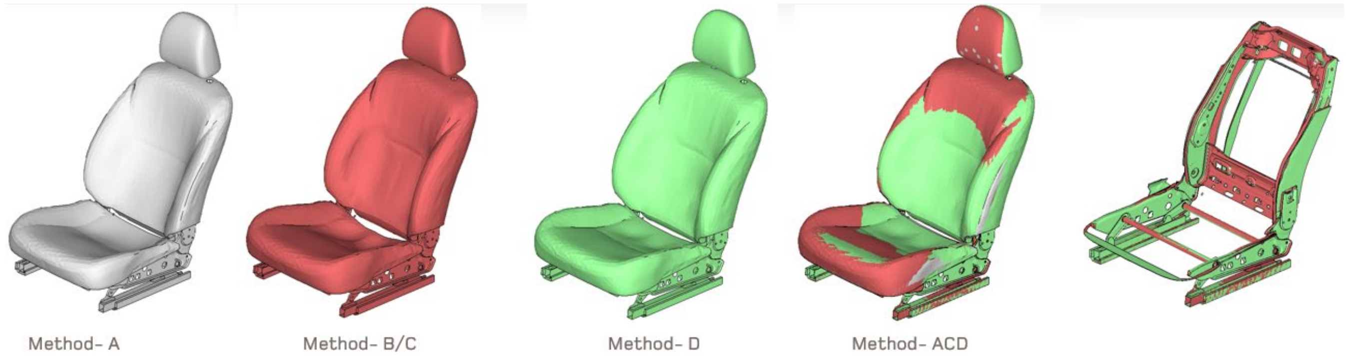

Fig. F1. HBM to seat interaction in all methods

The seat base cushion is more compressed in Method A, whereas Method B provides better impressions of the HBM bottom and back.

Seat penetration using the advanced Marionette method results in less seat compression than in methods A and B/C seats. In methods A, B and C, the rigid HBM is seated against the seat, whereas in method D the deformable HBM is seated against the seat.

The seat structure remains in the same position across all methods, whereas foam compression varies due to the different positioning methods.

Regarding Driver Airbarg (DAB) behavior, the volume and pressurbehaved similarly in all the simulations, as well as the head contact force, ensuring reproducible results.

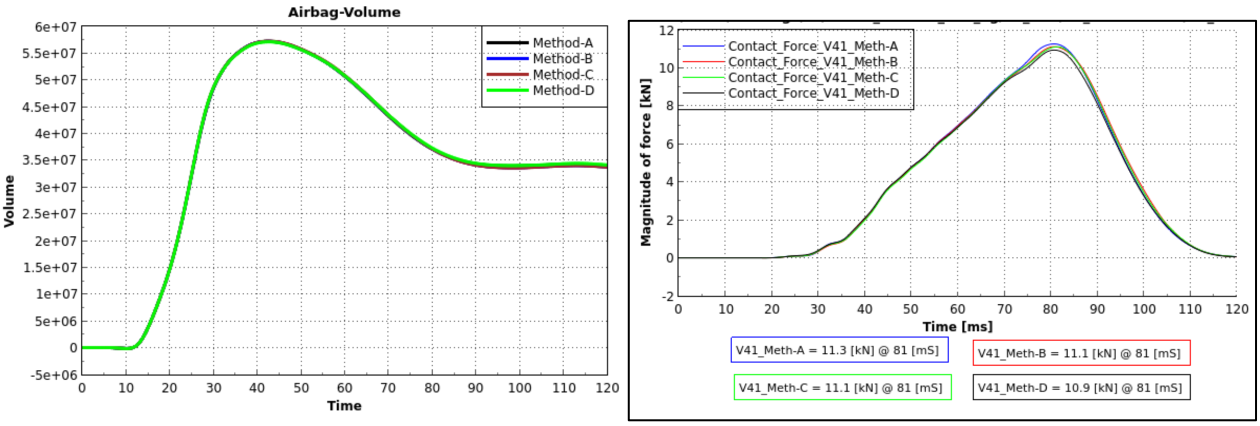

Fig. F2. DAB volume and Head to Airbag contact force across the four positioning methodologies.

Belt behavior and loading forces was similar across the four methods but some instabilities were observed in methods A and C in the interaction between the HBM and the lapbelt. The following image illustrates the noice capture in the lapbelt area, indicating that the mesh quality might have affected the performance of this contact.

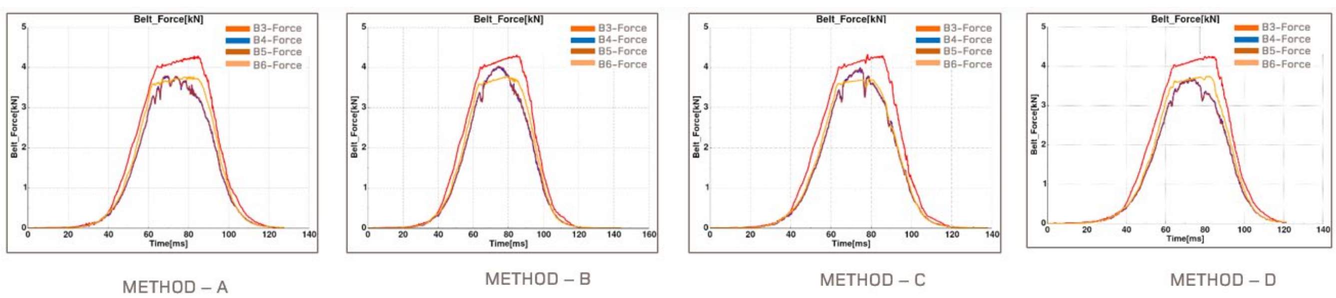

Fig. F3. Belt forces: behaviour of B4 and B5 forces show different noise in the signal between the different methods. A higher slip of the belt is observed in Method-C @75ms. B3 and B6 belt forces are almost equal in all the methods.